Pressure-tuned structure and electric transport properties in violet phosphorus

Wenjing Cheng,[1,*] Chenkai Li,[1,*] QunFei Zheng,[1] Jun Han,[1] Shanmin Wang,[1] Ying Liu,[1,†] and Jinlong Zhu[1,2,‡]

[1]*Department of Physics, Southern University of Science and Technology, Shenzhen 518055, China*

[2]*Quantum Science Center of Guangdong-Hong Kong-Macao Greater Bay Area (Guangdong), Shenzhen 518045, People's Republic of China*

(Received 17 February 2023; revised 11 May 2023; accepted 12 May 2023; published 22 May 2023)

Violet phosphorus, as a kind of two-dimensional material, has become an excellent candidate for optoelectronic devices as it makes up for the drawbacks of black phosphorus applications. This study explores the structural and electrical properties of violet phosphorus under high-pressure conditions. Two structure phase transitions are revealed by the spectra and electromagnetic transport measurements. At $\sim$ 8 GPa, a structural transition from monoclinic to A7 phase is observed with the appearance of superconductivity. The transition from the A7 phase to the simple cubic phase starts at $\sim$ 13 GPa and completes after $\sim$ 30 GPa at low temperatures. In addition, the band gap of violet phosphorus decreases linearly with the increase of pressure until it disappears after the transition to the A7 phase. The anisotropic upper magnetic field of superconductivities in A7 and simple cubic phases showed the relative crystal orientations of the high-pressure phases compared with initial violet phosphorus crystal phase.

DOI: 10.1103/PhysRevB.107.184513

I. INTRODUCTION

Ever since the discovery of graphene, there has been a growing interest in various two-dimensional materials like black phosphorus (BP) because of their exceptional photonic and electronic characteristics. BP is indeed a good candidate for nanoelectronics and nanophotonic devices because of its layer-dependent band gap [1], up to 1000 $cm^2\ V^{-1}\ s^{-1}$ carrier mobility and up to 10^5 on/off ratio [2]. However, the narrow band gap (ranging from 1.5 eV in the monolayer to 0.3 eV in bulk) of BP [3] and its instability in the environment [4] limits its application. Violet phosphorus (VP), which is considered the most stable allotrope of phosphorus, has recently been successfully synthesized [5]. VP has a larger band gap compared with BP, ranging from a direct band gap of 2.54 eV for the monolayer to an indirect band gap of 1.42 eV for the bulk state [5]. In addition, VP is predicted to have a hole carrier mobility of up to 3000–7000 $cm^2\ V^{-1}\ s^{-1}$, which is considered a candidate for flexible optoelectronic devices [6].

High pressure changes the distance between atoms in the crystal, resulting in changes in the crystal and electronic structure, and tuning physical properties on a macrolevel as well [7–11]. BP has proved that the band gap will close by applying hydrostatic pressure with a transition from semiconductor to conductor at $\sim$ 1.7 GPa [12]. Furthermore, BP undergoes structural phase transitions and shows superconductivity at low temperatures at higher pressures [13]. Furthermore, extensive research has been conducted on the phonon properties of VP under high pressures using Raman spectra. These studies have revealed that VP exhibits structural phase transitions similar to those observed in BP under high-pressure conditions [14]. However, the effect of pressure on the band structure and electrical properties of VP is underexplored.

In this work, the optical and electrical properties of high-quality VP single crystal have been systematically explored under high pressure. The results of Raman spectra, *in situ* ultraviolet-visible (UV-vis) absorption spectroscopy and electric transport measurements show that the VP stays at an insulating state before the structural phase transition, and the band gap of VP decreases linearly with the increase of pressure. At $\sim$ 8 GPa, VP undergoes a structural transition from monoclinic to A7 phase with an electronic structural transition to a metal state with superconductivity. The structural transition from A7 phase to the simple cubic (SC) phase starts at $\sim$ 13 GPa and completes at $\sim$ 30 GPa at low temperatures. Superconducting order parameters (anisotropy factor γ and coherence length ξ) and angle-dependent magnetoresistance were obtained from electromagnetic transport measurements at different pressures.

II. RESULTS AND DISCUSSION

Raman spectroscopy is widely used to study the evolution of vibration mode and structural transition of crystals under high pressure [7,11,13–18]. In this study, the structural information of VP single crystal under high pressure is determined through the Raman spectra, as shown in Fig. 1. At a pressure below $\sim$ 8 GPa the Raman spectrum of VP shows minimal changes except for a blueshift and a decrease in intensity. These observations suggest that the structure of VP remains stable within this pressure range [16–18]. When the pressure reaches $\sim$ 8 GPa, the characteristic peaks of VP disappear and are replaced by E_g mode ($\sim$ 308 cm^{-1}) and A_g^1 mode ($\sim$ 388 cm^{-1}) of A7 phase, which is also a high-pressure

*These authors contributed equally to this work.
†liuy37@sustech.edu.cn
‡zhujl@sustech.edu.cn

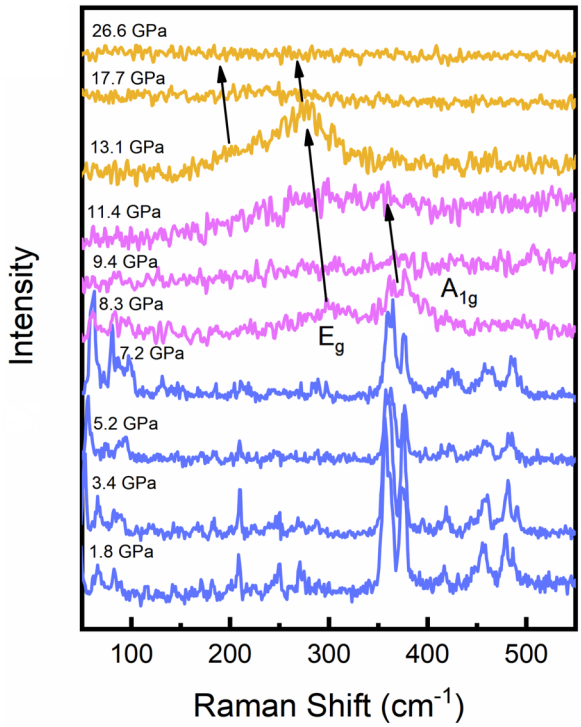

FIG. 1. Selected Raman spectra of VP under high pressure.

phase of BP [19]. The pressure of phase transition to A7 of VP (∼ 8 GPa) is significantly higher than the BP (∼ 5.5 GPa) [13]. This observation suggests that VP is considered to be in a more stable or "ground state" compared to BP [20]. After ∼ 13 GPa, A_g^1 mode disappears and a mode appears around 230 cm^{-1}, indicating the initiation of the transition from the A7 to the SC phase [19]. In fact, there is an intermediate stage of A7 + SC mixed-phase range from ∼ 13 to ∼ 30 GPa [21]. The pure SC structure appears after ∼ 30 GPa and is stable up to ∼ 100 GPa [22]. The existence of A7 + SC mixed phase was confirmed by x-ray diffraction measurements [21], and was also observed in the electromagnetic transport measurements in this work. The whole process of Raman spectra is consistent with the results reported by Zhang *et al.* [14].

To study the band-gap evolution as a function of pressure, the *in situ* UV-vis absorption spectroscopy was performed, as shown in Fig. 2. In Fig. 2(a), the absorption edge shows a significant redshift as the pressure increases to ∼ 8 GPa, and thereafter, the absorption edge disappears above ∼ 8 GPa. The

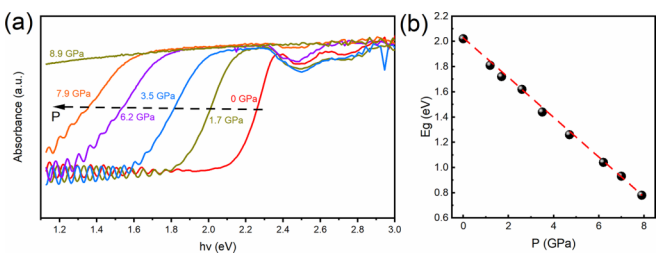

FIG. 2. (a) Selected *in situ* UV-vis patterns of VP under high pressure. (b) Band gap of VP under high pressure. [Dashed line gives out a slope of −0.155(2) eV/GPa].

pressure dependence of the band gap is shown in Fig. 2(b), which is determined using the Tauc method [23–25] (some examples of fitting are shown in Fig. S1 in Supplemental Material [26]). At ambient conditions, the indirect band gap is ∼ 2.02 eV, which is in line with the previous experimental and calculated results [27]. For a pressure less than 8 GPa, the band gap shows a linear reduction at 0.155(2) eV/GPa, compared with that of BP at 0.16–0.19 eV/GPa [12,28]. The reduction of the band gap is related to the increased band dispersion originating from the largely overlapped orbital, as the contractions of the bond and lattice are under pressure. When pressure is higher than 8 GPa, the band gap suddenly decreases to zero, showing an insulator-metal transition accompanying the monoclinic to A7 crystal structure phase transition [5,13]. On the other hand, BP achieves metallization under lower pressure (∼ 1.7 GPa) before a structural phase transition happened [12], and VP keeps high insulation (resistance larger than 200 MΩ) until it transforms to A7 phase.

To further explore the electrical properties of VP single crystal, the transport properties were measured through the Montgomery four-probe method [29,30] under high pressure. Figures 3(a) and 3(b) gives the photographic and schematic views of single-crystal VP in a diamond-anvil cell (DAC), respectively, and Fig. 3(c) shows the temperature (T) dependence of in-plane normalized resistance ($R/R_{300\,K}$) under different pressures and an inset plot of $R/R_{12\,K}$ vs T, ranging from 7 to 45 GPa (before 7 GPa, the resistance is over range). It is worth noting that a zero-resistance state appears at low temperatures above 7.6 GPa, indicating that superconductivity may occur. To confirm the superconductivity, a temperature dependence of the resistance under the magnetic field is performed, as shown in Fig. 3(d). As the magnetic-field strength rises, the superconducting transition temperature progressively decreases until the zero-resistance state vanishes and is replaced entirely by the normal resistance state. In addition, the critical magnetic field exhibits a clear dependence on the direction of the magnetic field. Specifically, when the magnetic field changes from perpendicular to parallel to the *ab* plane of the VP phase, distinct variations in the critical magnetic field are observed, as shown in Fig. 3(d).

Notably, superconducting critical temperature (T_c) shows an interesting double-dome shape with the increase in pressure, as shown in Fig. 3(e). In the A7 phase (before ∼ 13 GPa), a single dome-shaped pattern is observed. Initially, the superconducting transition temperature (T_c) increases with increasing pressure and reaches a peak of around 7 K at 9.5 GPa. Subsequently, T_c starts to decrease after reaching its peak. The dome shape of the T_c-P plot is common in pressure-tuned superconductivity [31–36]. According to the previous study that examined the high-pressure band structure and phonon frequency in the A7 phase [37], it was found that both the density of states at the Fermi energy [$N(\epsilon_F)$] and phonon frequency increase with the increase of pressure. These findings suggest that the increase in T_c observed in the A7 phase can be attributed to the corresponding increase in [$N(\epsilon_F)$] and phonon frequency. In addition, the decrease in T_c at higher pressure is related to possible structural instability [36,38]. For the second dome, the T_c reaches the maximum value of ∼ 9.6 K at ∼ 26 GPa in run 1 (∼ 9 K at ∼ 17 GPa in run 2). After ∼ 30 GPa, in the pure SC phase, T_c starts to

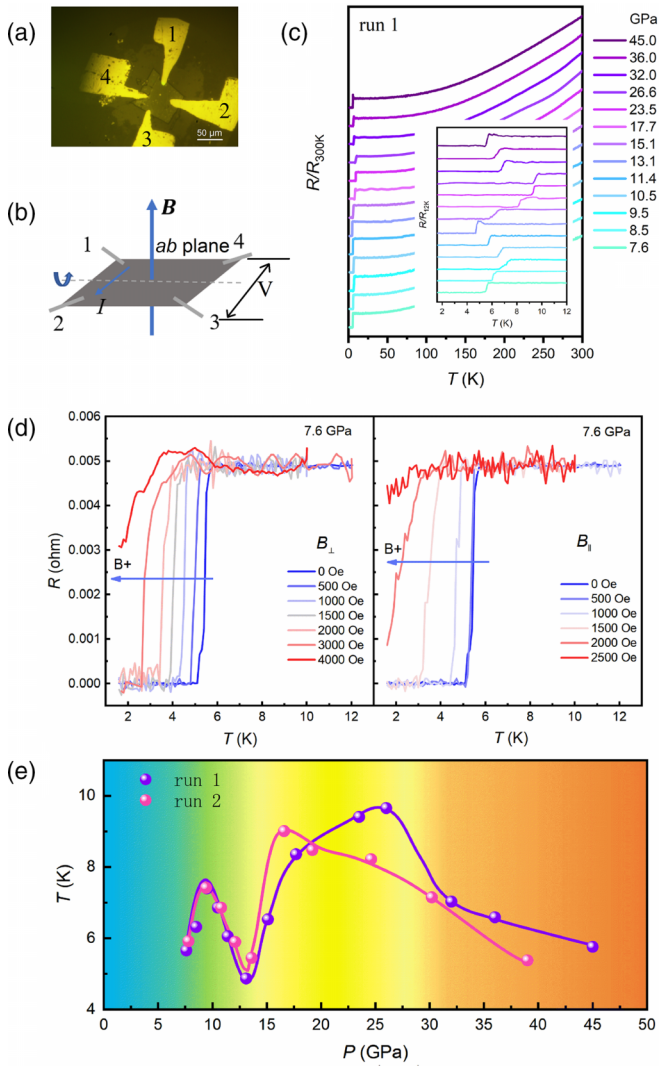

FIG. 3. (a) Photographic view and (b) schematic view of single-crystal VP in DAC and the arrangements of the electrode. (c) Temperature dependence of in-plane normalized resistance ($R/R_{300\,\mathrm{K}}$) of run 1 at different pressures with the inset plot of $R/R_{12\,\mathrm{K}}$ vs T ranging from 1.6 to 12 K of run 1. (d) Magnetic-field dependence of superconducting transition temperatures measured on the sample subjected to 7.6 GPa with field direction perpendicular (B_{90}) and parallel (B_0) to the sample plane. (e) T_c under high pressure under compression. In addition, the background color used to distinguish the structure of samples, blue, green, yellow, and orange correspond to the monoclinic phase, A7 phase, mixed phase, and SC phase in sequence.

decrease significantly with pressure. The second dome is similar to previous studies on BP [39]. According to a study by Chen *et al.*, the increase of T_c in the A7 + SC mixed phase ($\sim$ 13 to $\sim$ 30 GPa) can be explained by the increase in $N(\epsilon_F)$ and the decrease in T_c in the SC phase (after $\sim$ 30 GPa) is attributed to the weakening of electron-phonon coupling due to an increase in phonon frequency [38]. To confirm the reproducibility, T_c-P data obtained in run 2 are plotted in Fig. 3(e), which showed a similar double-dome shape. The $R/R_{300\,\mathrm{K}}$ and $R/R_{12\,\mathrm{K}}$ vs T plots are shown in Fig. S2 in Supplemental Material [26]. It is worth noting that the phase transition pressure from the mixed phase to the pure SC phase of run 2 is relatively low due to the difference in hydrostatic conditions. Moreover, gaining insights into the peculiar double-dome shape observed in the T_c-P plot could greatly benefit from conducting additional calculations on the electronic structure under high pressure. Specifically, investigating the dome observed in phase A7 would be particularly valuable in addressing this issue.

Moreover, the influence of carrier type on superconductivity is an important issue for superconductors. The Hall resistance (R_{xy}) under high pressure during run 2 was measured at 12 K and is plotted in Fig. S3 in Supplemental Material [26]. The slope of $R_{xy} - B$ is insufficient to obtain a reliable carrier type, which may be due to the carrier concentration being too high. The 'maximum slope is found at 16.6 GPa, showing the hole carriers with $\sim 1.3 \times 10^{22}$ cm^{-3}. Hence, it is apparent that hole carriers play a significant role in the advancement of superconductivity. However, the precise mechanism behind this phenomenon remains uncertain, emphasizing the necessity for additional experiments or calculations to verify and elucidate the underlying principles.

To study the anisotropic character of the different phases, an angular dependence of upper critical-field measurement of run 1 was performed. Figure 4 plots the upper critical field B_c versus angle θ [between the magnetic field and current shown in Fig. 3(b)] at 1.6 K. The upper critical field is closely related to the crystal orientation [33,40–45]. During the A7 phase, there is an observed positive correlation between the upper critical field and the angle. The maximum value is typically found at approximately 80° to 90°. The deflected position of maxima shows evidence of inclined crystal orientation with the c axis of the A7 phase oriented towards $\sim$ 80° to $\sim$ 90°, as shown in Fig. 4(a). Within the pressure range of approximately 13 to 30 GPa, corresponding to the mixed phase, the upper critical field demonstrates a distinct decrease. Moreover, it exhibits an unusual angle function characterized by an initial increase followed by a subsequent decrease. Notably, the maximum value occurs at approximately 50° to 70°. The observed pattern resembles a superposition of the behaviors exhibited by the A7 and SC phases. Specifically, the upper critical field in the A7 phase increases as the angle grows, while in the SC phase, it decreases with increasing angle. It strongly shows the existence of the A7 + SC mixing phase. As the pressure above $\sim$ 30 GPa (pure SC phase), the opposite phenomenon emerges where the upper critical field decreases as angle increases. Similar to cubic superconductor Nb [46–48], the direction of $\sim$ 90° is considered as the [001] direction (c axis), and the direction of 0° is considered as the [110] direction. Overall, the direction-dependent upper magnetic field is consistent with the phase transition and further outlines the relative crystal orientations of VP, A7, and SC phases, as shown in Fig. 4(d). It helps to further explore the kinetic process of these phase transitions.

The upper critical fields of the A7 phase, observed before reaching approximately 13 GPa, display the highest values and a notable anisotropic factor γ of up to approximately 1.9 at 7.6 GPa. However, as the pressure increases beyond that point, the anisotropic factor γ gradually decreases

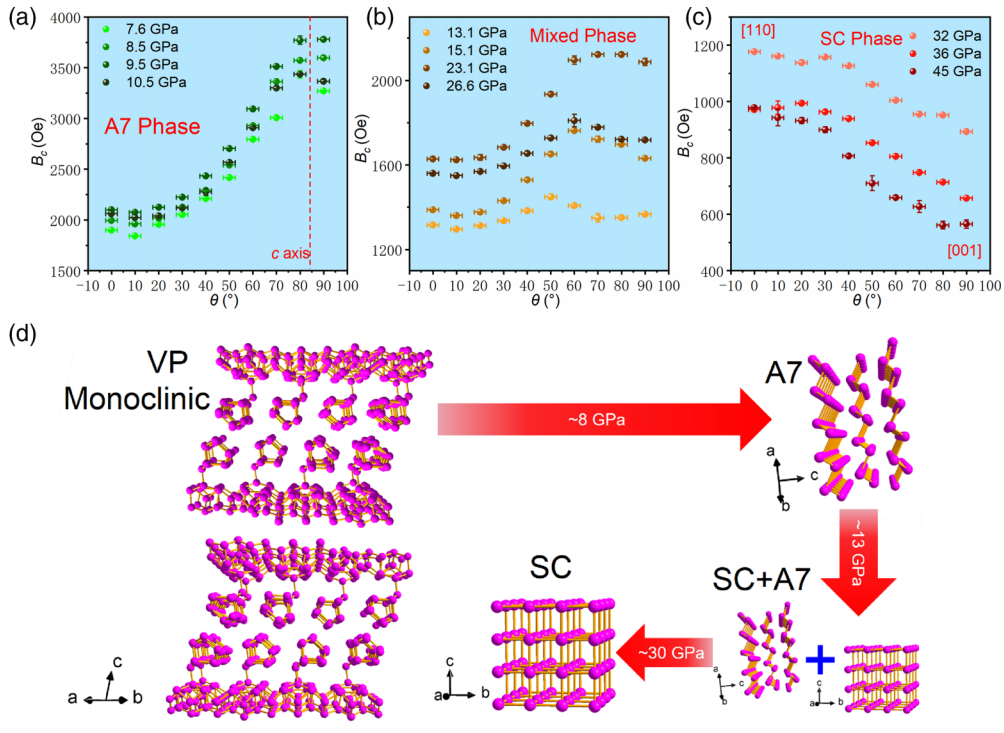

FIG. 4. Upper critical field measured at different angles and pressures at $T = 1.6$ K in (a) A7 phase, (b) mixed phase, and (c) SC phase. (d) Schematic diagram of the whole phase transformation process.

until reaching approximately 13 GPa, as shown in Fig. S4(d) in Supplemental Material [26] (see also Ref. [49] therein). In 2D superconductors, for bulk $Bi_{2.2}Sr_{1.9}CaCu_2O_{8+x}$ and $1T'-MoTe_2$, the anisotropic factor γ is found to be 40 and 2.1, respectively [40,43]. On the contrary, in 3D superconductors, for bulk $YBa_2Cu_3O_7$, $2H-NbSe_2$, and WTe_2, the anisotropic factor γ is nearly 8, 2.2, and 1.7, respectively [33,40–42]. The anisotropic factor γ of 1.9 shows that the superconductivity is possibly not confined within the block layer; rather, it exhibits a 3D character. In addition, the reduction of anisotropy is due to the transformation from layered materials (A7) into nonlayered materials (SC) beyond 30 GPa. The slight anisotropy in the SC phase is similar to another cubic structural superconductor Nb, whose anisotropy is attributed to Fermi-surface anisotropy [46–48].

III. CONCLUSIONS

In summary, the present study systematically explored the structure and electrical properties of VP single crystal under varying pressure. Two structure phase transitions appeared in VP evidenced by spectra and electromagnetic transport measurements. At ∼ 8 GPa, VP undergoes a structural transition from monoclinic phase to the A7 phase, and the transition from the A7 phase to SC phase starts at ∼ 13 GPa and completes after ∼ 30 GPa. The band gap of VP exhibits a linear decrease with increasing pressure until the transition to the A7 phase occurs. Superconductivity appeared in A7 and SC phases, as both were showing dome-shaped pressure dependence. The angle-dependent anisotropy outlined the relative crystal orientation where the c axis of the A7 phase showed an inclination of $80^\circ - 90^\circ$ degrees compared with the monoclinic phase, and it gradually became perpendicular in the SC phase to the *ab* plane of the VP phase.

IV. METHODS

Single crystals of VP used in this work were purchased from Nanjing MKNANO Tech. Co., Ltd. [50] (purity >99.9%). The pressure was generated by a DAC which has two opposite diamond anvils with a culet diameter of 300 μm. A symmetrical cell was used for UV-vis absorption spectra and a Be-Cu cell was used for transport measurements and Raman spectra. A T301 stainless-steel gasket, which was preindented to a thickness of 30 μm (the thickness of the T301 gasket before preindentation is ∼ 250 μm) and drilled a hole with a diameter of 200 μm, was used in different high-pressure studies. To maintain the hydrostatic pressure, Ar gas was used as the pressure-transfer medium (PTM) for UV-vis absorption spectrum measurements, and NaCl powder was used as the PTM for Raman spectra and transport measurements. The Montgomery four-probe method [29,30] was applied on the *ab* plane of single-crystal VP for the high-pressure transport measurements. The T301 gasket was insulated with c-BN powder for the transport measurements. The single-crystal sample was placed within the PTM. Subsequently, four electrodes made of Pt foil were positioned between the sample and the diamond anvil. The pressure is quantified by the displacement of ruby fluorescence lines [51].

Raman spectra were collected by a backscattering configuration using a microscope with an ∼ 5−μm focal point with a 532-nm laser and 1200-g/mm grating. To ensure the integrity of the sample, the laser power was set below 622 uW and the signal acquisition time was set to 60 s. The

UV-vis absorption spectrum was performed by the deuterium-halogen light source, and the absorption data were collected by the optical fiber spectrometer with a response time of 1 s.

ACKNOWLEDGMENTS

The work was supported in part by the National Key R&D Program of China Grant No. 2018YFA0305703, the National Natural Science Foundation of China Grants No. 12274193 and No. 12004161, the Stable Support Plan Program of Shenzhen Natural Science Fund under Grant No. 20200925152415003. J.Z. and Y.L. also acknowledge the Major Science and Technology Infrastructure Project of Material Genome Big-science Facilities Platform supported by Municipal Development and Reform Commission of Shenzhen. Some experiments are supported by the Synergic Extreme Condition User Facility. The authors express their gratitude to EditSprings [52] for the expert linguistic services provided.

[1] X. Ling, H. Wang, S. Huang, F. Xia, and M. S. Dresselhaus, Proc. Natl. Acad. Sci. USA **112**, 4523 (2015).
[2] L. Li, Y. Yu, G. J. Ye, Q. Ge, X. Ou *et al.*, Nat. Nanotechnol. **9**, 372 (2014).
[3] S. Lin, W. K. Lai, Y. Li, W. Lu, G. Bai, and S. P. Lau, SmartMat **2**, 226 (2021).
[4] J. D. Wood, S. A. Wells, D. Jariwala, K. S. Chen, E. Cho *et al.*, Nano Lett. **14**, 6964 (2014).
[5] L. Zhang, H. Huang, B. Zhang, M. Gu, D. Zhao *et al.*, Angew. Chem. Int. Ed. **59**, 1074 (2020).
[6] G. Schusteritsch, M. Uhrin, and C. J. Pickard, Nano Lett. **16**, 2975 (2016).
[7] C. Li, Y. Liu, Q. Yang, Q. Zheng, Z. Yan *et al.*, J. Phys. Chem. Lett. **13**, 161 (2022).
[8] X. Li, J. Sun, P. Shahi, M. Gao, A. H. MacDonald, Y. Uwatoko, T. Xiang, J. B. Goodenough, J. Cheng, and J. Zhou, Proc. Natl. Acad. Sci. USA **116**, 1065 (2019).
[9] C.-H. Li, Y.-J. Long, L.-X. Zhao, L. Shan, Z.-A. Ren, J.-Z. Zhao, H.-M. Weng, X. Dai, Z. Fang, C. Ren *et al.*, Phys. Rev. B **95**, 125417 (2017).
[10] Z. J. Xiang, G. J. Ye, C. Shang, B. Lei, N. Z. Wang *et al.*, Phys. Rev. Lett. **115**, 186403 (2015).
[11] Z. Chi, X. Chen, F. Yen, F. Peng, Y. Zhou *et al.*, Phys. Rev. Lett. **120**, 037002 (2018).
[12] Y. Akahama and H. Kawamura, Phys. Status Solidi B **223**, 349 (2001).
[13] X. Li, J. Sun, P. Shahi, M. Gao, A. H. MacDonald *et al.*, Proc. Natl. Acad. Sci. **115**, 9935 (2018).
[14] L. Zhang, H. Huang, Z. Lv, L. Li, M. Gu *et al.*, ACS Appl. Electron. Mater. **3**, 1043 (2021).
[15] X. Ren, X. Yan, A. S. Ahmad, H. Cheng, Y. Li *et al.*, J. Phys. Chem. C **123**, 15204 (2019).
[16] Z.-H. Chi, X.-M. Zhao, H. Zhang, A. F. Goncharov, S. S. Lobanov, T. Kagayama, M. Sakata, and X.-J. Chen, Phys. Rev. Lett. **113**, 036802 (2014).
[17] B. Han, F. Li, L. Li, X. Huang, Y. Gong *et al.*, J. Phys. Chem. Lett. **8**, 941 (2017).
[18] F. Li, Y. Yan, B. Han, L. Li, X. Huang *et al.*, Nanoscale **7**, 9075 (2015).
[19] G. Xiao, Y. Cao, G. Qi, L. Wang, Q. Zeng *et al.*, Nanoscale **9**, 10741 (2017).
[20] M. Aykol, J. W. Doak, and C. Wolverton, Phys. Rev. B **95**, 214115 (2017).
[21] J. Guo, H. Wang, F. von Rohr, W. Yi, Y. Zhou, Z. Wang, S. Cai, S. Zhang, X. Li, Y. Li *et al.*, Phys. Rev. B **96**, 224513 (2017).
[22] Y. Akahama, M. Kobayashi, and H. Kawamura, Phys. Rev. B **59**, 8520 (1999).
[23] P. Makuła, M. Pacia, and W. Macyk, J. Phys. Chem. Lett. **9**, 6814 (2018).
[24] A. L. Companion, in *Developments in Applied Spectroscopy*, edited by E. N. Davis (Springer US, Boston, MA, 1965), p. 221.
[25] P. Kubelka and F. Munk, Z. Tech. Phys. **12**, 593 (1931).
[26] See Supplemental Material at http://link.aps.org/supplemental/10.1103/PhysRevB.107.184513 for UV-vis spectra fitting examples by Tauc method of VP at selected representative pressures; temperature dependence of in-plane normalized resistance at different pressure of run 2; Hall measurements in 12 K at different pressure; temperature dependence of the upper critical field at 7.6 and 32 GPa with fitting lines; and pressure dependence of the upper critical field and anisotropy.
[27] Y.-L. Lu, S. Dong, W. Zhou, S. Dai, B. Zhou *et al.*, Phys. Chem. Chem. Phys. **20**, 11967 (2018).
[28] S. Huang, Y. Lu, F. Wang, Y. Lei, C. Song *et al.*, Phys. Rev. Lett. **127**, 186401 (2021).
[29] L. J. v. d. Pauw, Philips Res. Rep. **13**, 1 (1958).
[30] H. C. Montgomery, J. Appl. Phys. **42**, 2971 (1971).
[31] Y. Qi, P. G. Naumov, M. N. Ali, C. R. Rajamathi, W. Schnelle *et al.*, Nat. Commun. **7**, 11038 (2016).
[32] Y. Fang, Q. Dong, J. Pan, H. Liu, P. Liu *et al.*, J. Mater. Chem. C **7**, 8551 (2019).
[33] Y. T. Chan, P. L. Alireza, K. Y. Yip, Q. Niu, K. T. Lai, and S. K. Goh, Phys. Rev. B **96**, 180504(R) (2017).
[34] J. P. Sun, K. Matsuura, G. Z. Ye, Y. Mizukami, M. Shimozawa *et al.*, Nat. Commun. **7**, 12146 (2016).
[35] Z. Zhang, Z. Chen, Y. Zhou, Y. Yuan, S. Wang *et al.*, Phys. Rev. B **103**, 224513 (2021).
[36] X.-C. Pan, X. Chen, H. Liu, Y. Feng, Z. Wei *et al.*, Nat. Commun. **6**, 7805 (2015).
[37] J. A. Flores-Livas, A. Sanna, A. P. Drozdov, L. Boeri, G. Profeta, M. Eremets, and S. Goedecker, Phys. Rev. Mater. **1**, 024802 (2017).
[38] K. T. Chan, B. D. Malone, and M. L. Cohen, Phys. Rev. B **88**, 064517 (2013).
[39] M. Karuzawa, M. Ishizuka, and S. Endo, J. Phys.: Condens. Matter **14**, 10759 (2002).
[40] M. J. Naughton, R. C. Yu, P. K. Davies, J. E. Fischer, R. V. Chamberlin, Z. Z. Wang, T. W. Jing, N. P. Ong, and P. M. Chaikin, Phys. Rev. B **38**, 9280(R) (1988).
[41] N. Toyota, H. Nakatsuji, K. Noto, A. Hoshi, N. Kobayashi *et al.*, J. Low Temp. Phys. **25**, 485 (1976).
[42] Y. Muto, K. Noto, H. Nakatsuji, and N. Toyota, Nuovo Cimento B **38**, 503 (1977).

[43] Y. J. Hu, Y. T. Chan, K. T. Lai, K. O. Ho, X. Guo *et al.*, Phys. Rev. Mater. **3**, 034201 (2019).
[44] M. Tinkham, Phys. Rev. **129**, 2413 (1963).
[45] Y. Guo, J. Peng, W. Qin, J. Zeng, J. Zhao *et al.*, J. Am. Chem. Soc. **141**, 10183 (2019).
[46] D. E. Farrell, B. S. Chandrasekhar, and S. Huang, Phys. Rev. **176**, 562 (1968).
[47] P. C. Hohenberg and N. R. Werthamer, Phys. Rev. **153**, 493 (1967).
[48] H. W. Weber, E. Seidl, C. Laa, E. Schachinger, M. Prohammer, A. Junod, and D. Eckert, Phys. Rev. B **44**, 7585 (1991).
[49] J. A. Woollam, R. B. Somoano, and P. O'Connor, Phys. Rev. Lett. **32**, 712 (1974).
[50] G. Shen, Y. Wang, A. Dewaele, C. Wu, D. E. Fratanduono *et al.*, High Pressure Res. **40**, 299 (2020).
[51] www.mukenano.com.
[52] https://www.editsprings.cn.